Microsyst Technol (2008) 14:1185–1191
DOI 10.1007/s00542-008-0628-x

TECHNICAL PAPER

A novel method to fabricate single crystal nano beams with (111)-oriented Si micromachining

Heng Yang · Kefeng Xu · Yongliang Yang · Tie Li · Jiwei Jiao · Xinxin Li · Yuelin Wang

Received: 25 January 2008 / Accepted: 11 April 2008 / Published online: 1 May 2008
© Springer-Verlag 2008

Abstract Single crystal beams made by (111)-oriented Si micromachining are usually anchored to the substrate directly. It is difficult to use the beams as resonators, since they are electrically connected to the substrate. This paper presents a modified process to fabricate single crystal nano beams which are electrically isolated from the substrate. In this process, the single crystal nano beams are fully released from the substrate and mechanically supported by metal wires, which also serve as electrical connections. The metal wires are much stiffer than the beams and do not degrade the mechanical properties of the beam according to simulations. The length and width of the beams are determined by photolithography. The thickness of the beam and the gap between the beam and the substrate are determined by the dry etching and KOH etching processes. The influence of KOH etching on the beam thickness is documented through ongoing experiments. At present, the double clamped beams and the cantilever beams have been fabricated. The thinnest beam to date was measured to be 47 nm. The resistance between the beam and the substrate was measured to be 214GΩ, while the resistance of a 147 nm-thick beam was measured to be 816 Ω. The surface roughness of the (111) plane is also discussed. The RMS surface roughness of the nano beam was measured to be 1.08 nm in an area of 5 μm × 5 μm, which was etched with 45%wt. KOH at 50°C.

H. Yang (✉) · K. Xu · Y. Yang · T. Li · J. Jiao · X. Li · Y. Wang
National Laboratory of Microsystem Technology, Shanghai Institute of Micro System and Information Technology, Chinese Academy of Sciences, Changning Road 865, 200050 Shanghai, China
e-mail: h.yang@mail.sim.ac.cn

1 Introduction

Beams with nano thickness are the fundamental structures of many nano-electro-mechanical devices (Ekinci and Roukes 2005). Single crystal Si nano beams attract interest (Cleland and Roukes 1996; Erbe et al. 2001; Li et al. 2002) due to their excellent mechanical properties and lack of intrinsic strain and grain structures. Some methods have been developed to fabricate single crystal Si nano beams, most of which are based on SOI wafers (Erbe et al. 2001; Li et al. 2002).

Nano beams can also be made by anisotropic wet etching in standard (111) Si wafers (Pandraud et al. 2000; Oosterbroek et al. 2000; Cristea et al. 2005). The general process of (111) micromachining is illustrated in Fig. 1. After the structure shown in Fig. 1a is fabricated in a (111) Si wafer, it is etched with KOH. Since the etch rate of (111) planes is much lower than that of other planes, the KOH removes the silicon laterally and parallel to the (111) plane. The beam is formed after the underlying silicon is etched away, as shown in Fig. 1b. The thickness of the beam is approximately equal to that of the nano step in Fig. 1a, since the bottom of the beam is in the (111) plane, the etch rate of which is negligible. The nano step in Fig. 1a is formed by dry etching; its length and width are determined by photolithography. Thus, the length and the width of the nano beam are also determined by photolithography. The gap between the beam and the substrate is approximately equal to the depth of the trenches on both sides of the nano step in Fig. 1a; these trenches are formed by dry etching, and their depth can be quite accurately controlled. This allows for accurate fabrication of the finished nano-beam.

The drawback of the above method is that the beams are electrically connected to the substrate, making it difficult to use them in devices. We have modified the process to

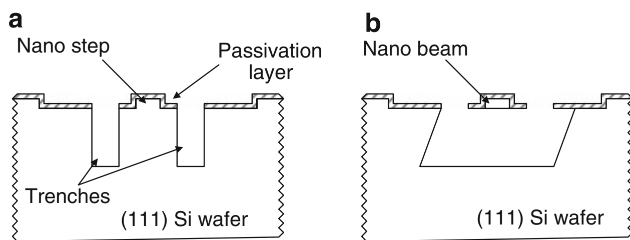

Fig. 1 Fabrication of a free standing structure in (111) Si wafers

fabricate single crystal Si beams with nanometer thickness that are isolated from the substrate, as shown in Fig. 2. Instead of anchoring to the substrate, the beams are mechanically supported by metal wires, which also serve as electrical connections. Since the metal wires are much stiffer than the Si beams, the resonant frequency of the whole structure is determined by the Si beam. The length and the width of the beams are determined by photolithography. The thickness of the beams is approximately determined by the dry etching, which can be accurately controlled. The gaps between the beams and the substrates are also determined by the dry etching. Both double clamped beams and cantilever beams have been fabricated by this method.

The resonant frequencies of the nano beam structures are analyzed in Sect. 2. The experiments and the results of the nano beam fabrication are discussed in Sect. 3. Some other issues including surface roughness and etching of the nano beams are discussed in Sect. 4.

2 Resonant frequencies

When the metal wires are much stiffer than the silicon nano beam, the fundamental resonant frequency of the whole structure shown in Fig. 2 is approximately equal to that of the nano beam, which can be estimated with Rayleigh-Ritz methods. For the double clamped silicon nano beam and the silicon cantilever, the fundamental resonant frequencies are (Bao 2000):

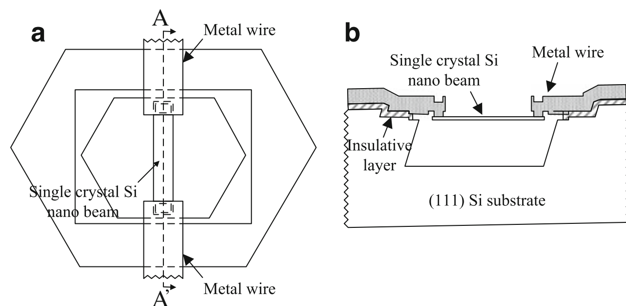

Fig. 2 The nano beam supported by metal wires. **a** Top view. **b** Cross sectional view on the AA' plane

$$f_{b0} = 1.03 \frac{h_b}{L_b^2} \sqrt{\frac{E_{Si}}{\rho_{Si}}} \quad (1)$$

$$f_{c0} = 0.16 \frac{h_b}{L_b^2} \sqrt{\frac{E_{Si}}{\rho_{Si}}} \quad (2)$$

where h_b is the thickness of the nano beam, L_b is the length of the nano beam, E_{Si} is the Young's modulus of Si, and ρ_{Si} is the density of Si.

When the Si beam is much thinner than the metal wires, it is reasonable to assume that the metal wires act as cantilevers. The fundamental resonant frequency of the metal wire can also be estimated with the Rayleigh–Ritz method:

$$f_{M0} = 0.16 \frac{h_M}{L_M^2} \sqrt{\frac{E_M}{\rho_M}} \quad (3)$$

where h_M is the thickness of an Au wire, L_M is the length of the wire, E_M is the Young's modulus of Au, and ρ_M is the density of Au.

For the double clamped beam shown in Fig. 2, the structure must fulfill the relation: $f_{bo} < f_{mo}$ or:

$$\frac{h_b}{L_b^2} \frac{L_M^2}{h_M} < 0.155 \sqrt{\frac{E_M}{E_{Si}} \frac{\rho_{Si}}{\rho_M}} \quad (4)$$

For the cantilever beam, the structure must fulfill the relation: $f_{c0} < f_{M0}$ or:

$$\frac{h_b}{L_b^2} \frac{L_M^2}{h_M} < \sqrt{\frac{E_M}{E_{Si}} \frac{\rho_{Si}}{\rho_M}} \quad (5)$$

When relation (4) or (5) is fulfilled, the fundamental resonant frequency of the metal wire determines a higher harmonic frequency of the whole structure.

Finite element simulations agree with the analysis above. Figure 3 shows the first three resonant frequencies of a double clamped nano beam, as extracted by ANSYS. The nano beam is 32 μm × 3 μm × 100 nm and is supported by two Au wires. Each of the Au wires is 20 μm × 3 μm × 2 μm. The first resonant frequency of the structure as extracted by ANSYS is 859 kHz, while the resonant frequency of the Si nano beam as calculated by Eq. 1 is 860 kHz. The second and third simulated resonant frequencies of the structure are 1.63 and 1.81 MHz, while the resonant frequency of the Au wire as calculated by Eq. 3 is 1.62 MHz. The deviations of the second and third resonant frequencies from the fundamental frequency of the Au wire are caused by coupling between the fundamental frequency of the Au wire and the second and third resonant frequencies of the Si nano beam.

Simulations for the cantilevers also match well with the theory. An example is a single crystal Si beam measuring 32 μm × 3 μm × 100 nm, supported by an Au wire

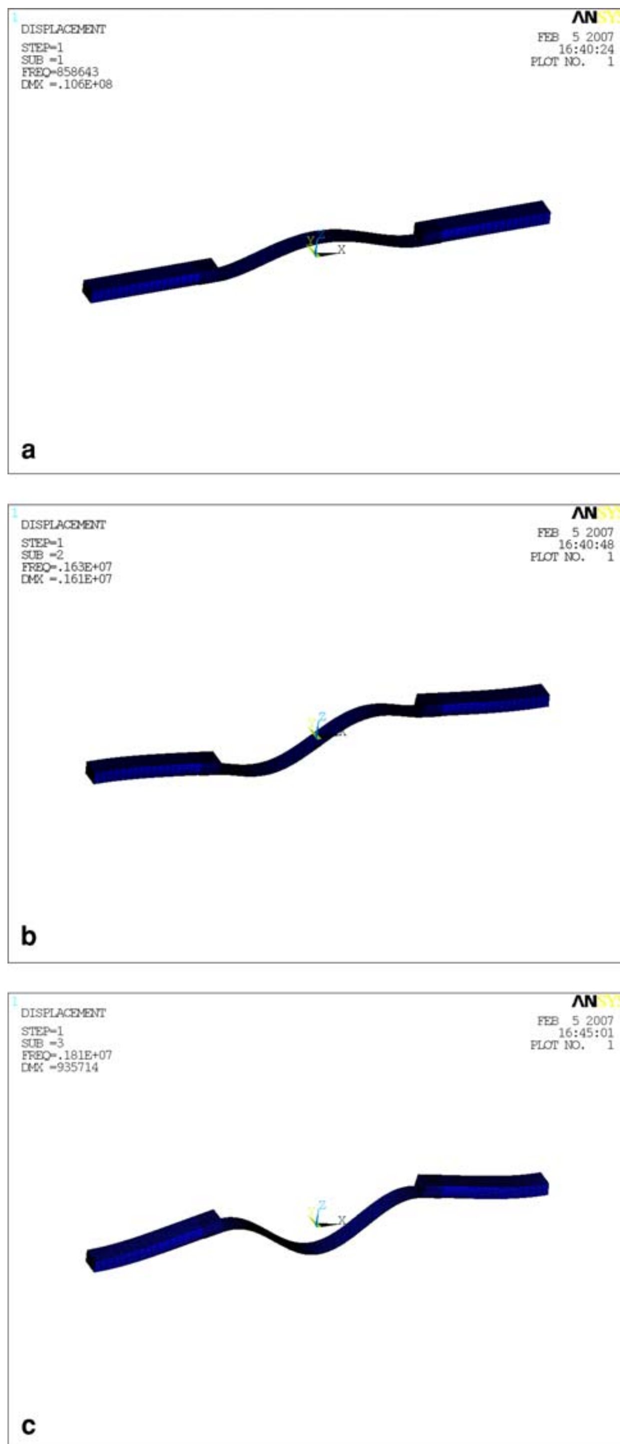

Fig. 3 The first three resonant frequencies of a double clamped nano beam as extracted by ANSYS

measuring 20 μm × 3 μm × 2 μm. The first simulated resonant frequency of the structure is 135 kHz, while the value obtained by Eq. 2 is 134 kHz. The second resonant frequency of the structure is approximately equal to the second resonant frequency of the Si beam. The Au wire determines the third resonant frequency of the structure; the simulated frequency is 1.64 MHz, and the frequency calculated from Eq. 3 is 1.62 MHz.

3 Fabrication and results

The wafers used in the experiments were 4-inch *n*-type (111) wafers with 0° ± 1° deviation from (111) orientation. The resistivity was 35–45 Ω cm. The fabrication process is described below and illustrated in Fig. 4.

(1) As the surfaces of the (111) wafers deviated slightly from the (111) plane, the application of a KOH pre-etching was needed to expose the (111) plane (Pandraud et al. 2000; Oosterbroek et al. 2000). An oxide layer of 4,000 Å thickness was thermally grown to serve as the mask for KOH etching. After the etch windows were patterned, the wafers were etched in 45%wt. KOH at 50°C for 13 h to expose the (111) plane. The top view and the cross-sectional view of the sample after the KOH etching are shown in Fig. 4a. The final shape of the (111) plane was usually hexagonal, regardless of the shape of the window before the KOH etching. The etch window for pre-etching was kept as small as possible in order to control the planarity. The rate of exposure of the (111) plane was determined by the orientation of the wafers and the etchants. More than 10 h were required to expose the (111) plane of a 100 μm × 100 μm etch window in 50°C 45%wt. KOH. The surface roughness of the (111) planes obtained by wet etching may have important effects on the properties of the nano-beams, since the thickness of the beams was comparable with the surface roughness (Alan et al. 2006). Since the surface roughness increases with temperature and decreases with increases in concentration, 45%wt. KOH at 50°C was used.

(2) After the entire oxide layer was stripped with HF, the beam was defined by reactive ion etching. The etching depth was 870 nm. Boron was then diffused, followed by thermal growth of a 2500 Å oxide layer to passivate the sidewalls and the surface of the beam, as shown in Fig. 4b. The sheet resistance was measured to be 74 Ω^2.

(3) After the contact holes were opened, seed layers were sputtered. Both Cr/Au and TiW/Au seed layers were used in the different experiments. The layer of Cr or TiW was 1,000 Å thick, while the layer of Au was 2,000 Å thick. A layer of 10 μm photoresist was spun on and patterned to serve as the electroplating mold. The Au wires were electroplated to 5 μm with a commercial non-cyanide plating solution, as shown in

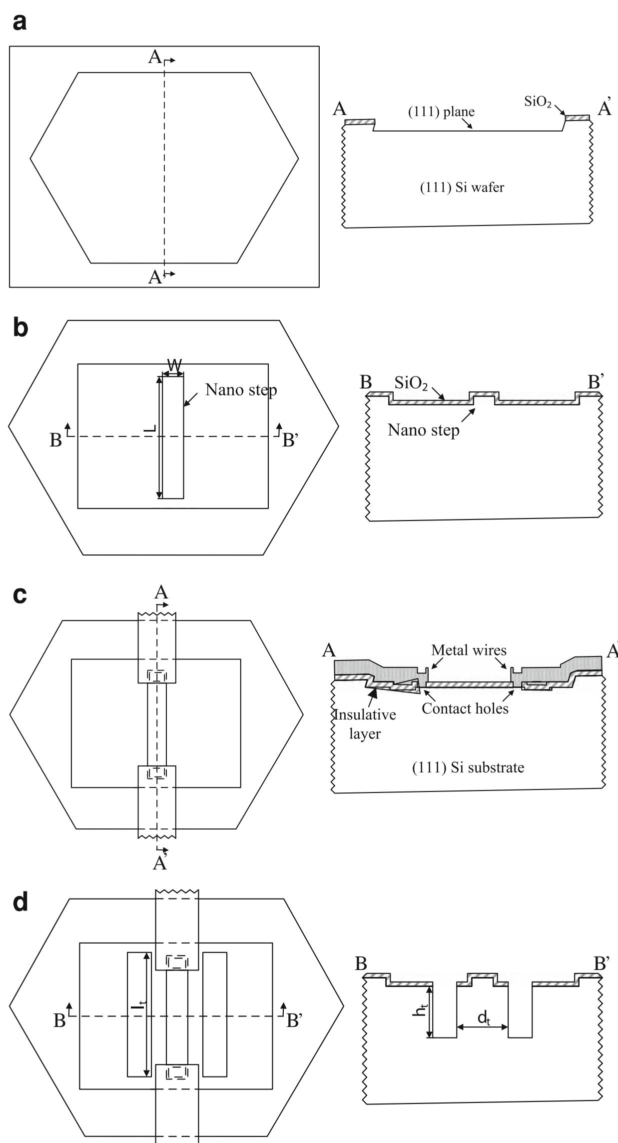

Fig. 4 The process flow of the nano beam on the (111) wafer. *Top views* and *cross-sectional views* are shown. The structure after KOH etching is shown in Fig. 2. **a** KOH pre-etching was applied to expose the (111) plane. **b** Nano steps were defined by dry etching. The etching depth was 870 nm. Boron was diffused. A layer of 2,500 Å SiO_2 was thermally grown to passivate the sidewalls and the surface of the beam. **c** The contact holes were opened. Seed layers were sputtered. The Au wires were electroplated to 5 μm. The seed layer was removed by dry etching. **d** The trenches were patterned and etched by ICP

Fig. 4c. Au was used because it can withstand KOH etching. The photoresist was stripped with acetone and the seed layer was removed.

(4) Spray coating instead of spin coating was used to coat the photoresist uniformly. The trenches were patterned and etched by reactive ion etching, as shown in Fig. 4d. The initial gap between two trenches, d_t, must fulfill the relation in (6) to release the beam properly:

$$d_t < (2h_t \tan\alpha + l_t)\tan 30^\circ \quad (6)$$

where l_t, w_t and h_t are the length, width and depth of the trenches, and α is the angle between the (111) side wall and the bottom. This angle is calculated to be 70.53° based on the relationships between the (111) planes. Different etch depths were used in the experiments, including 5 μm, 10 μm and through-wafer.

(5) The wafer was etched in 45%wt. KOH at 50°C for 7 h to release the beam. The profiles of the trenches on both sides of the beam changed with KOH etching, as shown in Fig. 5. The solid line in Fig. 5a shows the profile before the two trenches merge. The moving rate of the edges parallel to the x-direction was measured to be 4.5 μm/h in 50°C 45%wt KOH. The dotted line in Fig. 5b shows the profile after the two trenches merge. The etch rates of the left and the right convex corners were not equal due to the asymmetry of the Si crystal structure; they were measured to be 4.87 and 6.93 μm/h, respectively, in 50°C 45%wt KOH. The final profile, obtained by the principle of (111) etching, is shown in solid lines in Fig. 5(b). All of the exposed Si surfaces were (111) planes. The final length of the trench in the x-direction was calculated based on the relationships between the (111) planes.

$$l_b = h_t \tan\alpha + l_t \quad (7)$$

(6) The structure shown in Fig. 2 was obtained after the SiO_2 layer was etched away by HF. Since the gaps were large, the samples were dried with nitrogen after rinsing in water. Supercritical drying was unnecessary in our cases.

Figure 6 shows the SEM of a double clamped beam structure. The thickness of the beam was measured to be 147 nm from Fig. 6b, as the sample tilt was 80°. When the gaps between the beams and the substrate were 10 μm, more than 70% of the structures withstood the etching and the drying processes. Figure 7 shows the AFM picture of the surface of a beam. The RMS roughness was measured to be 1.08 nm in an area of 5 μm × 5 μm. The current-voltage relations of the structure in Fig. 8 were measured with an Agilent 4156. Fig. 8a, b show the I–V relations within the nano beam, and between the beam and the substrate, respectively. The resistance of the beam was 816 Ω when the voltage was 1 V. The resistance between the beam and the substrate was 214 GΩ when the voltage was 1 V. Thermal annealing was not required to obtain the ohmic contact when a TiW/Au seed layer was used. Figure 9 shows the SEM picture of a cantilever structure.

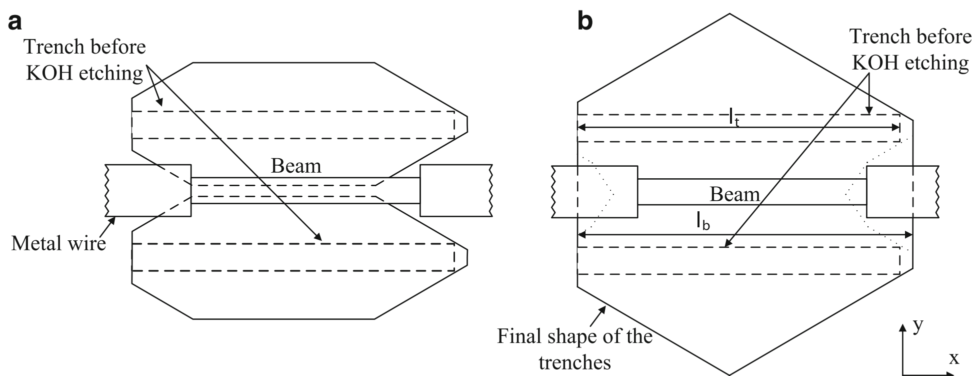

Fig. 5 The profiles of the trenches on either side of the beam change with the KOH etching. **a** The profiles before the two trenches merge. **b** The profiles after the two trenches merge

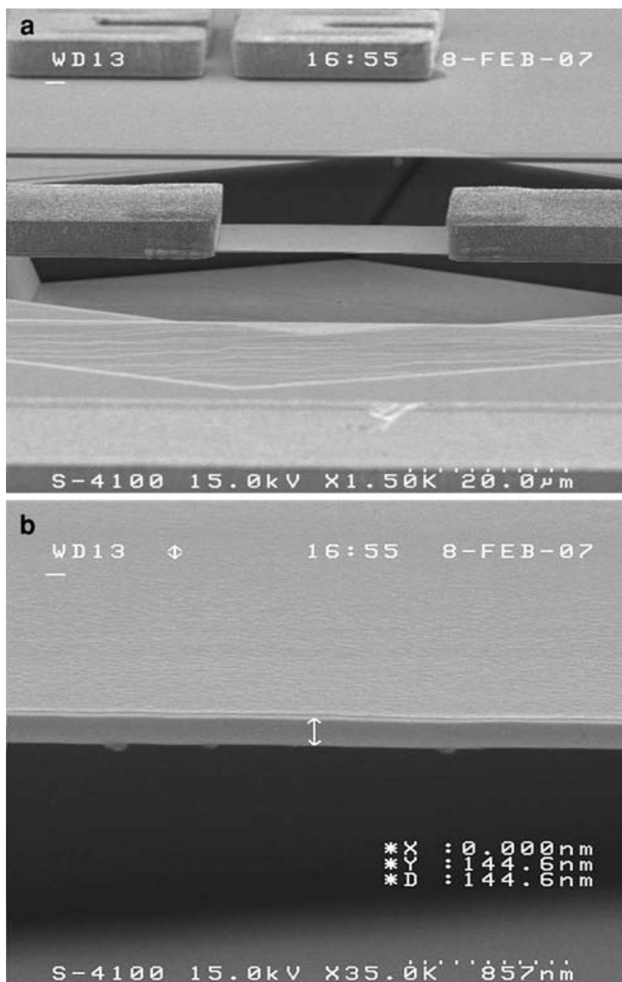

Fig. 6 The double clamped nano beam supported by Au wires. The beam is 32 μm long, 20 μm wide and 147 nm thick. The Au wires are 5 μm thick. The gap between the beam and the substrate is about 10 μm. **a** A double clamped nano beam supported by Au wires. **b** Close-up of the beam

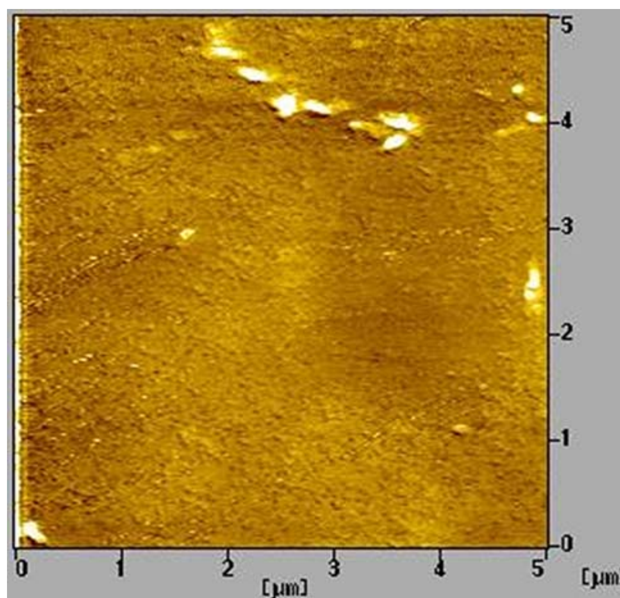

Fig. 7 AFM picture of a beam surface. The RMS roughness is 1.08 nm in an area of 5 μm × 5 μm

4 Discussion

4.1 Surface roughness

Experiments were performed to determine the surface roughness in different etchants at different temperatures. The wafers used in the experiments were 4-inch n-type (111) wafers with 0° ± 1° deviation from the (111) plane. The KOH solution was mixed using AR-grade KOH powder and deionized water. As the concentration of KOH in the solid powder was 82%, the 45%wt. KOH solution was mixed using 55%wt. powder and 45%wt. water. After a layer of 4000 Å SiO_2 was thermally grown, 100 μm × 100 μm windows were patterned. The samples were dipped in 3.6% HF for 15 s and dried with nitrogen. They were then etched in KOH until the thickness of SiO_2 decreased to less than 500 Å. The concentrations of KOH were 33, 37, 41 and 45%wt. The surface roughness was measured in an area of 5 μm × 5 μm by AFM. Figure 10 shows the surface roughness as a function of the KOH concentration and temperature. The experimental results indicate that high concentration and low temperature are preferred in order to obtain smooth surfaces.

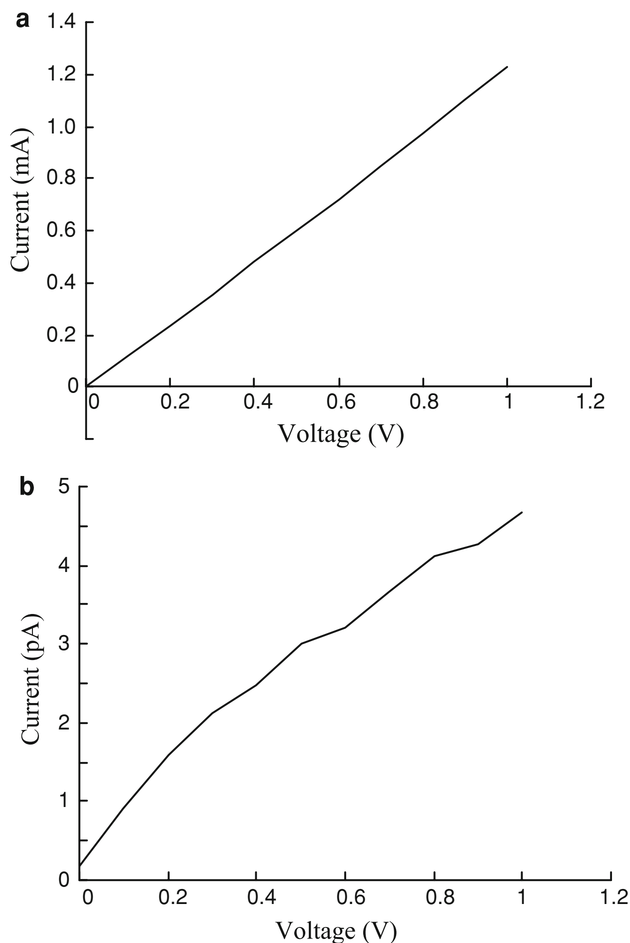

Fig. 8 IV relations. a IV relation of the nano beam. b IV relation between the beam and the substrate

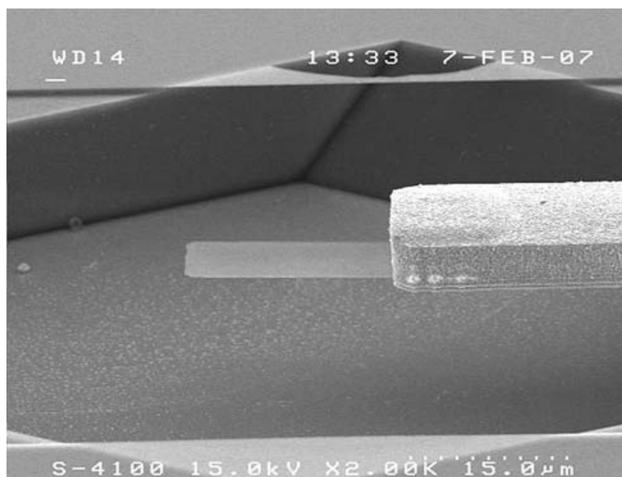

Fig. 9 SEM picture of a cantilever structure

4.2 Etching of the nano beams

In principle after the nano beams are released, their etch rates should become negligible since their bottom surfaces

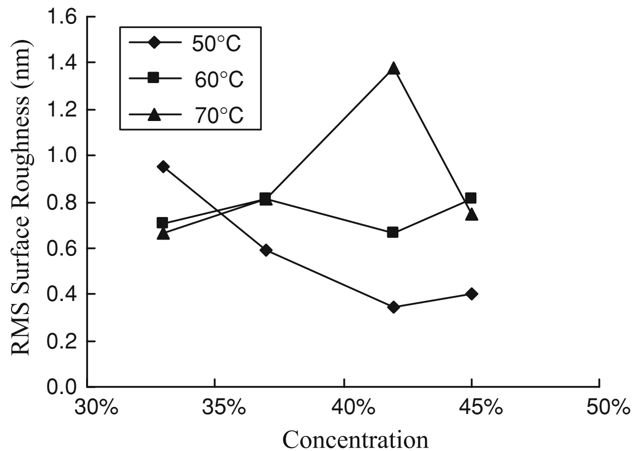

Fig. 10 RMS surface roughness with respect to temperature and concentration

are (111) planes. In the experiments, however, the initial etch rate was much faster than that of a (111) plane. Figure 11 shows the thicknesses of the beams versus etch time. Since it was difficult to track the thickness of a single sample, six samples were etched with different etch times. The solution was 45%wt. KOH at 50°C. The initial thickness was 870 nm, while the thickness after 2 h of etching was measured to be 353 nm. The fast initial etch rate was considered to be caused by the nonuniformity of dry etching. The final etch rate of the bottom surface of the beam was estimated to be 38 nm/h. As the etch rate of the (100) plane was measured to be 3.6 μm in the same solution at 50°C, the etch rate ratio between the (100) and the (111) plane was 95:1. The nano step should initially be defined with greater than the desired thickness with dry etching, in order to compensate for the nonuniformity caused by the dry etching. The compensation value must be determined experimentally.

The beams can be thinned further with KOH etching. The very low etch rate provides for good control of the

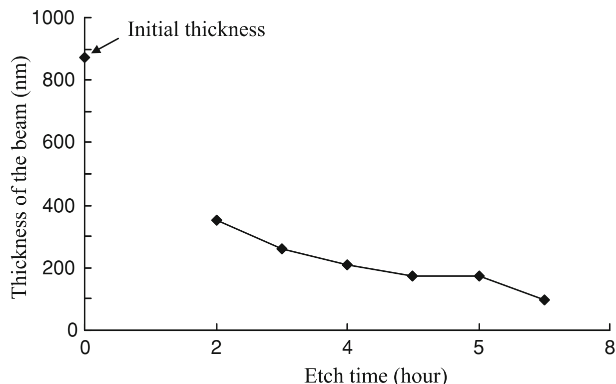

Fig. 11 The thickness of the beams changes with KOH etching. Data were obtained using six samples

Fig. 12 The thinnest beam to date was 47 nm thick. The sample tilt was 79°

thickness. The thinnest beam to date measured 47 nm, as shown in Fig. 12.

5 Conclusions

We have presented a novel method to fabricate single crystal Si nano beams in standard (111) wafers. As the beams are mechanically supported by metal wires, they are electrically isolated from the substrate. The resistance between a beam and the substrate was measured to be 214 GΩ. The metal wires also served as electrical connections. Simulations showed that the metal wires do not degrade the resonant frequencies of the Si nano beams, as the wires are much stiffer than the beams. Double clamped nano beams and nano cantilevers have been fabricated. The thickness of a double clamped beam was measured to be 147 nm. The thinnest beam to date was 47 nm. More than 70% of the double clamped nano beams withstood the etching and drying processes without special drying techniques. Surface roughness versus concentration and temperature of KOH was measured, indicating that high concentration and low temperature are preferred to obtain smooth surfaces. The RMS surface roughness of a nano beam was measured to be 1.08 nm in a 5 μm × 5 μm area.

Acknowledgments This work is partly supported by the National Basic Research Program of China "Micro-to-nano scale fabrication based on top-down principle (Project 2006CB300403).

References

Alan T, Hines MA, Zehnder AT (2006) Effect of surface morphology on the fracture strength of silicon nanobeams. Appl Phys Lett 89:091901

Bao MH (2000) Micro mechanical transducers-pressure sensors, accelerometers, and gyroscopes. Elsevier, Amsterdam

Cleland AN, Roukes ML (1996) Fabrication of high frequency nanometer scale mechanical resonators from bulk Si crystals. Appl Phys Lett 69:2653–3655

Cristea C, Kusko M, Tibeica C, Muller R, Manea E, Syvridis (2005) Design and experiments for tunable optical sensor fabrication using (111)-oriented silicon micromachining. Sens Actuators A113:312–318

Ekinci KL, Roukes ML (2005) Nanoelectromechanical systems. Rev Sci Instrum 76:061101

Erbe A, Weiss C, Zwerger W, Blick RH (2001) Nanomechanical resonator shuttling single electrons at radio frequencies. Phys Rev Lett 87:096106

Li X, Ono T, Wang Y, Esashi M (2002) Study on ultra-thin NEMS cantilevers—high yield fabrication and size-effect on Young's modulus of silicon. The 5th Int. Conf. on micro electro mechanical system IEEE, Las Vages, USA, pp 427–430

Oosterbroek RE, Berenschot JW, Jansen HV, Nijdam AJ, Pandraud G, van den Berg A, Elwenspoek MC (2000) Etching methodologies in ⟨111⟩-oriented silicon wafers. J MEMS 9:390–398

Pandraud G, Veldhuis G, Berenschot JW, Nijdam AJ, Hoekstra HJWM, Parriaux O, Lambeck PV (2000) Micromachining of high-contrast optical waveguides in ⟨111⟩ silicon wafers. IEEE Photon Tech Lett 12:308–310